Thermal stability of a magnetic domain wall in nanowires

S. Fukami,[1,2,*] J. Ieda,[3] and H. Ohno[1,2,4,5]

[1]*Center for Spintronics Integrated Systems, Tohoku University, 2-1-1 Katahira, Aoba, Sendai 980-8577, Japan*

[2]*Center for Innovative Integrated Electronic Systems, Tohoku University, 468-1 Aramaki Aza Aoba, Aoba, Sendai 980-0845, Japan*

[3]*Advanced Science Research Center, Japan Atomic Energy Agency, Tokai, Ibaraki 319-1195, Japan*

[4]*Laboratory for Nanoelectronics and Spintronics, Research Institute of Electrical Communication, Tohoku University, 2-1-1 Katahira, Aoba, Sendai 980-8577, Japan*

[5]*WPI Advanced Institute for Materials Research, Tohoku University, 2-1-1 Katahira, Aoba, Sendai 980-8577, Japan*

(Received 20 July 2014; revised manuscript received 11 May 2015; published 4 June 2015)

We study the thermal stability of a magnetic domain wall pinned in nanowires with various widths and thicknesses made of Co/Ni multilayers and analyze the effective volume that governs the thermal stability. We find that, above a critical wire width, the domain wall depinning is initiated by a subvolume excitation and that the critical width is dependent on the wire thickness. The obtained findings are supported by the distribution of critical current density for domain wall depinning and are qualitatively described by an analytical model in which the balance between the Zeeman energy and domain wall elastic energy is considered. We also show a different behavior between the device size dependence of the thermal stability and that of critical current, leading to an enhancement of domain wall motion efficiency with decreasing the device size.

DOI: 10.1103/PhysRevB.91.235401 PACS number(s): 85.75.Dd, 75.60.Ch, 75.78.Fg

I. INTRODUCTION

Ferromagnets are used for their nonvolatility, i.e., an ability to retain the magnetization direction against external disturbance without a power supply, with which one can design nonvolatile random access memories and logic devices as well as hard disk drives [1,2]. The nonvolatility of a magnetic device is characterized by an energy barrier E between two stable configurations and is often measured in units of k_BT as the thermal stability factor E/k_BT, where k_B is the Boltzmann constant and T the absolute temperature; an E/k_BT of 40 is required to ensure 10 years' retention of one bit and the required value increases to about 70 for large-scale memories [3]. For ferromagnetic elements, the E is generally proportional to the product of saturation magnetization M_S, a critical magnetic field H_C, and a volume V. Consequently, when one reduces the element dimension in order to enhance the areal density and performances such as operation power and speed, the E/k_BT degrades because of the decrease in V. It has also been shown that there is a length scale for nucleation reversal above which exchange stiffness and the thickness of the material governs E, particularly in the case of perpendicular-easy-axis magnetic tunnel junction (MTJ) devices having a diameter of more than 30–40 nm [4,5]. In this context, it is of great interest, from not only fundamental but also technological points of view, to clarify the factor governing E and its dependence on the thickness and lateral size down to deep sub-100 nm. The thermal stability of a magnetic domain wall (DW) formed in nanowire is also characterized by the E/k_BT, which, in this case, represents how stable the DW can stay at a certain position, or how easily the DW is depinned from a pinning site under thermal fluctuation. This is not only a general problem in condensed matter and statistical physics, but it is also an issue of importance for applications to current-induced DW-motion [6] devices, which have been proposed and have gathered considerable interest [7–9]. The DW depinning induced by electric current [10–15] or thermal fluctuation [16–21] has been studied, and E for depinning with adiabatic spin-transfer torque generated by the spin-polarized current has been found to be different from that with thermal fluctuation [19,20]. However, physics and the nature of the E/k_BT involved in the DW motion and its scaling relation with respect to the device size and thickness have not been elucidated. In particular, while a few studies have been carried out to characterize thermally assisted DW depinning using continuous films or micrometer-sized wires [16–18,21–26], E/k_BT at the nanoscale dimension with various thicknesses along with the current-induced DW-motion properties relevant for nonvolatile devices has not been clarified.

In this study we investigate the thermal stability of a DW formed at an artificially prepared pinning site in nanometer-sized wires with various widths and thicknesses in order to address the physics that governs the E/k_BT. In addition to thermal stability, we evaluate the width and thickness dependence of the critical current density J_C to drive the DW and discuss its relation with the E/k_BT.

II. EXPERIMENTS

Co/Ni multilayers with a perpendicular magnetic easy axis are used throughout this work, in which a well-defined DW motion driven by an adiabatic spin-transfer torque has been observed [12,15,19,20]. The films are deposited by dc-magnetron sputtering onto high-resistivity 3-inch Si wafers. The stack structure is, from the substrate side, Ta(3 nm)/Pt(2 nm)/[Co(0.3 nm)/Ni(0.6 nm)]$_N$/Co(0.3 nm)/Pt(1.5 nm)/Ta(3 nm). The stacking number of the Co/Ni bilayer N is varied from 2 to 6, corresponding to a magnetic layer thickness t_{mag} from 2.1 to 5.7 nm. From measurements of the magnetization hysteresis loop along the out-of-plane and in-plane directions, the M_S and effective perpendicular anisotropy energy density K_{eff} are found to decrease from 0.97 to 0.94 T and from 0.26 to 0.14 MJ/m^3, respectively, as

*s-fukami@csis.tohoku.ac.jp

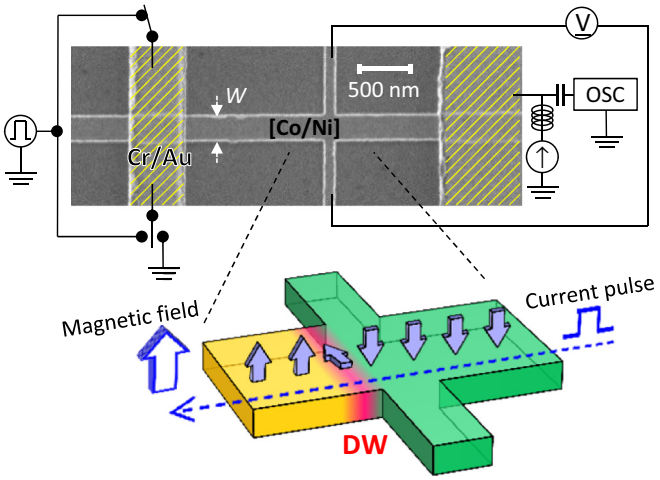

FIG. 1. (Color online) Scanning electron micrograph and schematic illustration of a fabricated device with measurement circuit. DW is prepared at the Hall cross, and current pulses or external fields are applied. The anomalous Hall effect is used to detect whether the DW is moved across the Hall cross.

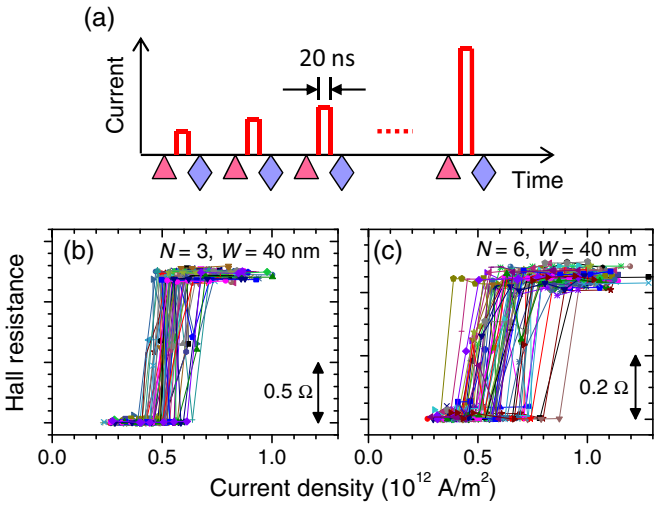

FIG. 2. (Color online) Measurement of current-induced domain wall depinning. (a) Measurement sequence. DW is initialized, and Hall resistance is measured at times indicated by red triangles and blue diamonds, respectively. Hall resistance versus current density of applied pulse for 80 devices with $W = 40$ nm and (b) $N = 3$, and (c) $N = 6$.

N increases from 2 to 6. The deposited films are patterned into nanowires with a pair of Hall probes by electron-beam lithography and Ar ion milling, on which Cr/Au electrodes are formed by electron-beam lithography and liftoff. The nominal widths W of fabricated nanowires in which DW moves are 20, 30, 40, 60, 80, 120, 160, and 240 nm, and those of the Hall probe W_H, are designed to be 20, 20, 20, 30, 40, 60, 80, and 120 nm, respectively. The resistance of wires shows that the width of fabricated wires is equal to the nominal ones within ±3.3%. The total number of devices fabricated on a wafer is 960; 120 devices for each W. In Fig. 1, a scanning electron micrograph of a fabricated device with $W = 240$ nm is shown together with the measurement circuit. To evaluate E/k_BT and J_C, we first prepare a DW at the Hall cross (initialization) and then apply dc magnetic fields or current pulses, as shown in the schematic illustration in Fig. 1 [15]. The anomalous Hall resistance R_H is measured to examine the DW depinning across the Hall cross with a dc current density of less than 5×10^{10} A/m^2. Note here that R_H is found to be independent of W, indicating that M_S is independent of W in the studied range.

III. RESULTS

A. Current-induced DW motion

Before evaluating the thermal stability, we first characterize the properties of the DW motion of fabricated samples induced by current pulses. The measurement sequence is depicted in Fig. 2(a). We apply 20-ns pulsed currents with various amplitudes I to the nanowires followed by subsequent measurement of R_H. Prior to every pulse application, the sample is initialized. 80 devices are measured for each W. Figures 2(b) and 2(c) show examples of measured R_H versus current density J for the 80 devices with $W = 40$ nm and $N = 3$ and 6, respectively. Here, J denotes the current density flowing in the Co/Ni multilayer, which is calculated from the current flow ratio determined by measuring the sheet resistance of separately prepared films with various stack structures. For all devices, R_H changes from low to high levels as I increases as a result of DW motion. The J_C, defined as the smallest J by which the R_H changes to the high level, is around 5×10^{11} A/m^2, which is consistent with the previous works [12,15,19,20].

Figure 3(a) shows J_C as a function of W for $N = 3$, 4, and 6. Plots and error bars denote the average (ave) and standard deviation (σ_{J_C}) of J_C obtained from the 80 devices. For all N, J_C shows a minimum with respect to W, as was seen in a previous study [12]. This originates from the dependence of hard-axis anisotropy on W [27]. It should also be noted that W giving the minimum J_C depends on N, i.e., it is 70 nm for $N = 3$, 50 nm for $N = 4$, and 30 nm for $N = 6$.

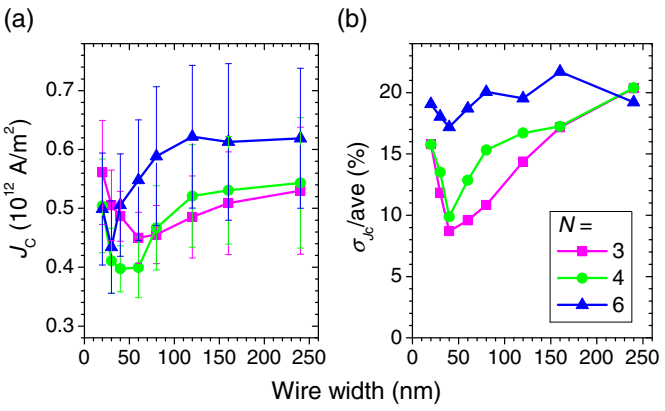

FIG. 3. (Color online) Width and thickness dependence of current-induced domain wall depinning properties. (a) Critical current density J_C and (b) the ratio of the standard deviation to average σ_{J_C}/ave as a function of wire width for various stack numbers N.

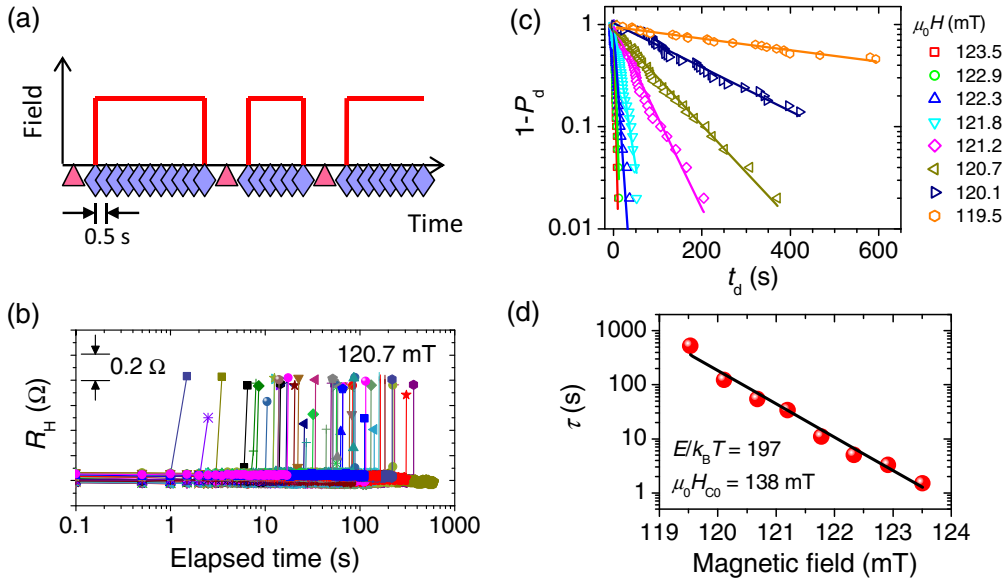

FIG. 4. (Color online) Evaluation of thermal stability factor E/k_BT and intrinsic critical field H_{C0}. (a) Measurement sequence. Indications of red triangles and blue diamonds are the same as those in Fig. 2(a). (b) Variation in Hall resistance R_H with time under an external field of 120.7 mT for a device with $W = 20$ nm and $N = 4$. (c) Cumulative probability of not depinning $1 - P_d$ versus depinning time t_d under various magnitudes of magnetic field. (d) Characteristic depinning time τ versus magnetic field. Inset shows the values of E/k_BT and $\mu_0 H_{C0}$ derived from fitting.

This reflects the width at which a DW changes its magnetic structure between the Bloch and Néel walls and its dependence on t_{mag}, as was also shown in the theoretical study [27]. While theoretical studies revealed that in the Bloch wall region J_C decreases with t_{mag} [27,28], our experimental results show that J_C of $N = 3$ and 4 are almost the same. We also note that the DW motion was not observed below $J \sim 1 \times 10^{12}$ A/m^2 in a number of devices with $N = 2$. These can be attributed to the low effective spin polarization of thin Co/Ni layers sandwiched by Pt [29] or nonvanishing spin-orbit torques [30]. Figure 3(b) shows the standard deviation of J_C divided by the average σ_{J_c}/ave, which represents the bit-to-bit distribution of J_C as a function of W. As can be clearly seen in Figs. 2(b) and 2(c), the bit-to-bit distribution of J_C is much larger for samples with larger N. The implication of the distribution of J_C with various W and N is discussed later in its relation to thermal stability.

B. Thermal stability of DW

We now turn to thermal stability. The thermal stability factor E/k_BT is evaluated by measuring the depinning time t_d under various magnetic fields H. The measurement sequence is depicted in Fig. 4(a). After the initialization, a dc magnetic field is applied and R_H is measured at a constant interval (0.5 s) up to 600 s, until R_H changes abruptly due to the DW depinning. We repeat this sequence 50 times for each value of H. Figure 4(b) shows the time variation of R_H under $\mu_0 H = 120.7$ mT for a device with $W = 20$ nm and $N = 4$. In this case, t_d ranges from 1.5 to more than 600 s. The cumulative probability of DWs being not depinned, 1-P_d, is shown as a function of t_d for various H in Fig. 4(c). For the majority of devices (95% of tested ones) on which we focus here, $1 - P_d$ is well described by the Néel-Brown model and fitted by an exponential function, $1 - P_d = \exp(-t_d/\tau)$, indicating that a single energy barrier governs the depinning with a characteristic depinning time τ. Then the obtained τ is plotted as a function of H [Fig. 4(d)]. The value of τ is expressed as $\tau = \tau_0 \exp\{E/k_BT \cdot (1 - H/H_{C0})\}$, where H_{C0} is the intrinsic critical field in the absence of thermal activation [20,31]. By fitting this equation to the experimental results, E/k_BT and H_{C0} are determined. For the case shown in Fig. 4(d), E/k_BT and $\mu_0 H_{C0}$ are 197 ± 9 and 138 ± 6 mT, respectively. In this work, three devices for each W with $N = 2$, 4, and 6 are measured, and their E/k_BT and H_{C0} are derived.

The average values of E/k_BT and H_{C0} are shown in Figs. 5(a) and 5(b), respectively. E/k_BT slightly increases as W and N decrease. H_{C0} is independent of N and proportional to $1/W$; the latter is consistent with the previous reports [25,26]. If we assume that V is proportional to W and N, we expect E/k_BT to be constant with W and be proportional to N, because E is proportional to the product of M_S, H_{C0}, and V, with H_{C0} being proportional to $1/W$ and independent of N, the change in M_S regarding N and W being negligible. However, this is not what we see in the present experimental result, particularly when W is greater than 70 nm.

IV. DISCUSSION

A. Effective volume of DW

The slight increase in E/k_BT with decreasing W suggests that there is an effective volume governing the E/k_BT of DW, V^* hereafter, that does not correspond to the geometric volume. Also, the decrease in E/k_BT with increasing N from 2 to 6 suggests that V^* is smaller for thicker samples. Such a subvolume effect is generally seen in a creep motion of DW. In [17], an effective volume was determined from the size at which the DW dynamics was deviated from the elastic creep motion in two dimensions using micro- and

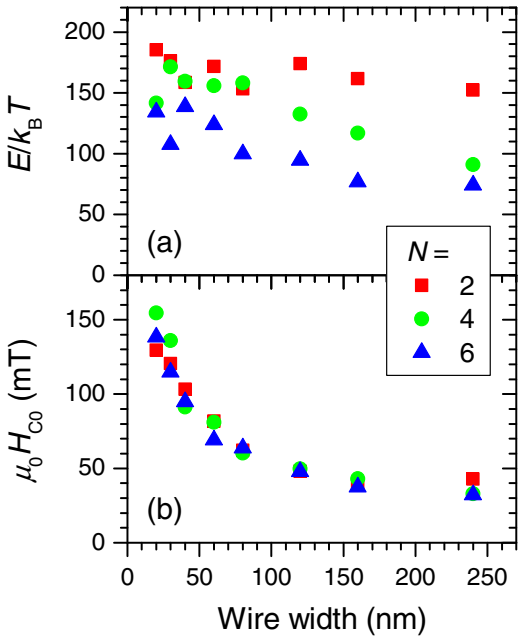

FIG. 5. (Color online) Width and thickness dependence of E/k_BT and $\mu_0 H_{C0}$. (a) E/k_BT and (b) $\mu_0 H_{C0}$ versus wire width for various stack numbers N. Each plot denotes average value obtained from three devices.

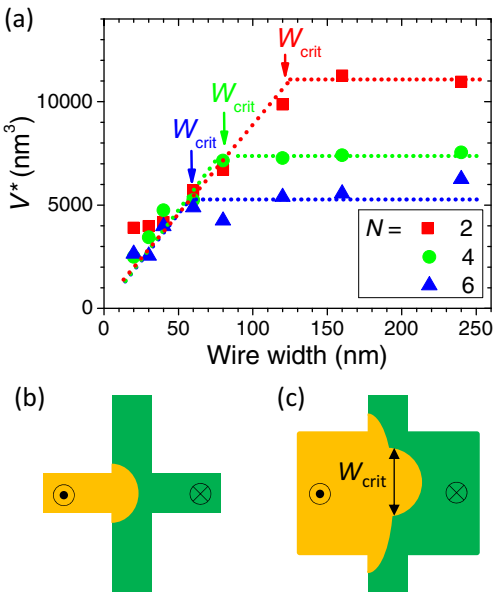

FIG. 6. (Color online) (a) Effective volume V^* that governs E/k_BT versus wire width for various stack numbers N. Schematic illustration of DW depinning in which (b) the whole volume of DW moves coherently and (c) partial volume, subvolume, with the width of W_{crit} triggers the depinning.

submicrometer-sized wires. Let us examine the value of V^* in the present case. An analytical study on magnetic bubble material showed that E for DW can be expressed as $2M_S H_{C0} V^*$ [32], which was confirmed by experimental studies [24,25]. The V^* can then be derived from the measured M_S, H_{C0}, and E/k_BT with $T = 300$ K, which is shown in Fig. 6(a). Interestingly, V^* initially increases with increasing W up to a critical width W_{crit}, above which it is almost constant, as shown by the dotted lines. This means that E/k_BT is governed by the DW volume defined by the device dimension below W_{crit} and above which only a portion of DW, i.e., the subvolume, with the length scale of W_{crit} contributes to E/k_BT, as illustrated in Figs. 6(b) and 6(c), respectively. This is analogous to the case with the MTJ device, in which E/k_BT is dominated by a subvolume for device diameters larger than the DW width, below which the geometrically defined volume of MTJ governs the E/k_BT factor [4,5]. Another notable fact is that W_{crit} appears to depend on N, that is, W_{crit} decreases as t_{mag} increases. This indicates that an incoherent DW depinning, i.e., depinning triggered by the subvolume as depicted in Fig. 6(c), becomes more likely as the thickness increases. It is also noteworthy that the devices that do not follow the Néel-Brown picture (about 5% of tested ones) are more frequently observed for larger W and N. This fact reinforces the above findings, because the deviation from the Néel-Brown picture implies that the DW is more likely to depin through multiple energy paths with stochastic subvolume excitation [16]. We can calculate the effective area S^* and effective length L^* of DW governing E/k_BT, as $S^* = V^*/t_{mag}$ and $L^* = S^*/W_H$ [25], leading to several thousands of nm^2 and several tens of nm, respectively; these are within the expected range from our device geometry. We also note that the obtained value of W_{crit}, which increases to more than 100 nm as t_{mag} decreases to 2.1 nm, is roughly consistent with the previous report [17], where critical width below which the elastic creep nature is missed was determined to be ~300 nm in a CoFe wire with $t_{mag} = 0.3$ nm.

B. Relation of effective volume with current-induced DW-motion properties

Now we discuss the effect of such a subvolume excitation on the bit-to-bit distribution of J_C. We previously found that the bit-to-bit distribution of J_C, σ_{Jc}/ave, is dominated by the self-distribution within one device, except for a very narrow region less than about 40 nm, where process-induced factors become dominant. The distribution was revealed to originate from the two-dimensional (2D) degree of freedom of the DW configuration [33], i.e., the DW forms a winding shape in 2D space and can contain Bloch lines which cause the bit-to-bit distribution. In this regard, σ_{Jc}/ave should closely link to V^* because V^* also relates to the 2D degree of freedom of the DW configuration. Let us look at Fig. 3(b) again and compare it with Fig. 6(a). We see that above 40 nm, σ_{Jc}/ave decreases with decrease of W, indicating that, as the wire width reduces, the 2D degree of freedom becomes more limited, and the DW is unlikely to form a winding shape during the motion, leading to the suppression of depinning by subvolume excitation. This is consistent with the observation of W_{crit} in Fig. 6(a). The decrease in σ_{Jc}/ave of the samples with smaller N starts from a wider region, indicating that the 2D degree of freedom of the DW configuration is reduced and the DW tends to move more coherently, as shown in Fig. 6(b), as the wire thickness decreases. This is also in accordance with the suggestion obtained from the analysis shown in Fig. 6(a), where W_{crit} increases as N decreases. Also, for $N = 6$, σ_{Jc}/ave does not decrease with W in Fig. 3(b), suggesting that the 2D degree

of freedom does not decrease down to around $W = 40$ nm. This is also consistent with the observed W_{crit} for $N = 6$ in Fig. 6(a) (≈50 nm). Overall, the variation in σ_{Jc}/ave with W and N supports our experimental findings that W_{crit} exists and it decreases as N, or t_{mag}, increases.

C. Analytical model

Next we discuss what determines W_{crit} and why W_{crit} becomes larger for a smaller t_{mag} using an analytical model. DW is depinned with a subvolume at $W > W_{crit}$ because the energy cost is lower than the coherent process. Previous studies on the depinning process at the Hall cross revealed that the DW could be treated as a soap bubble in 2D space [24,25]. In this case, we should consider the change in the Zeeman energy ε_Z and the DW elastic energy ε_{DW}, where the former and latter are proportional to the change in volume δV of the domain and area δS of the DW, respectively, brought about by the external field application. For simplicity, we here assume that a semicircle-shaped DW soap bubble with a diameter $\hat{W}$ is formed as shown in Fig. 6(c) under a magnetic field H, and consider the total energy $\varepsilon_{tot}(= \varepsilon_Z + \varepsilon_{DW})$ as a function of $\hat{W}$. The gain of ε_Z is given by $\pi M_S H \hat{W}^2 t_{mag}/4$, whereas the loss of ε_{DW} is given by $(\pi - 2)\sigma_{DW}\hat{W}t_{mag}/2$, where σ_{DW} is the DW energy density per unit area given by $4\sqrt{AK_{eff}}$ (A is the exchange stiffness constant) [34]. The bubble can appear only when $\partial\varepsilon_{tot}/\partial\hat{W} < 0$. [If $\partial\varepsilon_{tot}/\partial\hat{W} > 0$, the DW is depinned coherently as shown in Fig. 6(b).] Thus the critical diameter of the bubble, corresponding to W_{crit} in the present model, can be given by $\partial\varepsilon_{tot}/\partial\hat{W} = 0$, and the energy barrier E for the bubble-triggered depinning can be given by ε_{tot} at $\hat{W} = W_{crit}$, leading to $W_{crit} = (\pi - 2)\sigma_{DW}/\pi M_S H$ and $E = (\pi - 2)^2\sigma_{DW}{}^2 t_{mag}/4\pi M_S H$. Although the expression of W_{crit} does not explicitly depend on t_{mag}, it contains σ_{DW} ($\propto \sqrt{K_{eff}}$), which is a decreasing function of t_{mag} in our samples, as mentioned earlier. When we input experimental values, it leads to the decrease of W_{crit} by 26% with increasing N from 2 to 6, qualitatively consistent with our observation where W_{crit} decreases by 50% as N increases from 2 to 6 [Fig. 6(a)]. As for E/k_BT, while t_{mag} increases 300%, the present model leads to the increase of E ($(\propto \sigma_{DW}{}^2 t_{mag})$ by only 49%; the experimental result shows a slight decrease with increase in N from 2 to 6 [Fig. 5 (a)]. As described here, the present analytical model reasonably explains our experimental results. The residual discrepancy may be attributed to factors like the shape of the excited subvolume (instead of a semicircle, we find better agreement with the experiment, which is shown in Appendix) and/or thickness dependence of A.

We also note the difference between the present analysis and the one reported recently [21], in which a model that explains Barkhausen jumps of a DW activated by a laser-induced local heating has been put forward. In the model, the DW has been treated as a point particle, whereas it is treated as an elastic object in ours. In the present case, where the DW is under the presence of a magnetic field, a contribution of δV on the total energy has to be considered. This makes it necessary for us to take the effect of subvolume into consideration, eventually resulting in the scaling relation derived above.

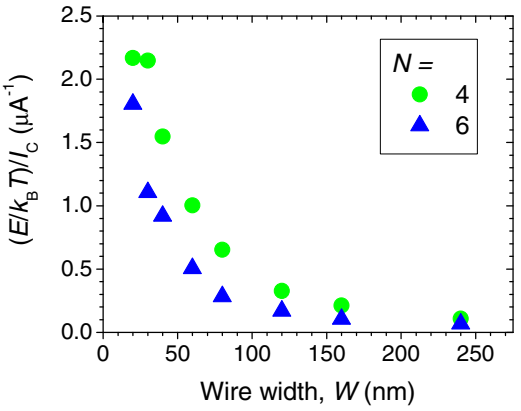

FIG. 7. (Color online) DW-motion efficiency ($(E/k_BT)/I_C$) versus wire width for $N = 4$ and 6 calculated from obtained E/k_BT [Fig. 5(a)] and I_C [Fig. 3(a)].

D. DW-motion efficiency

Lastly, we discuss the technological significance of the present study. At dimensions less than W_{crit}, I_C almost linearly scales with W, whereas E/k_BT stays almost constant. Parenthetically, J_C depends on W due to the dependence of hard-axis anisotropy on W; the variation in J_C with W is much less dominant than the decrease in cross-sectional area with W. Thus the efficiency of DW motion ($\eta \equiv \{E/k_BT\}/I_C[\mu A]$) increases almost inversely proportional to W, as shown in Fig. 7. The efficiency becomes more than 2 at $W \approx 20$ nm, which is greater than the macrospin limit of the spin-transfer torque switching ($\eta \approx 1$) of MTJs [5]. Note that I_C and E/k_BT of the MTJ device scale in the same manner with respect to the device size in principle, leading to a size-independent efficiency [4,5], which is in stark contrast to the DW-motion device. Furthermore, the increase in H_{C0} with the decrease in W means that robustness to external magnetic fields is enhanced by reducing the device size. In this regard, magnetic nanowire memory devices with current-induced DW motion have a promising characteristic in terms of device size reduction. In addition, no degradation of E/k_BT with the decrease of t_{mag} is a bright prospect for devices that use spin-orbit torques [13,14], because a thin magnetic layer is desirable in these devices.

V. CONCLUSIONS

The thermal stability of DW in nanowires made of Co/Ni multilayers with various W and N is studied. We find that E/k_BT slightly increases as W and N decrease, while H_{C0} is proportional to $1/W$ and is independent of N. By deriving the effective volume V^* that governs E/k_BT from them, we find a critical width W_{crit} above which the DW depinning is initiated with a subvolume excitation. The value of W_{crit} is larger for thinner wires. The findings regarding W_{crit} are supported by the variation in bit-to-bit distribution of J_C with W and N, and qualitatively explained by an analytical model where Zeeman and DW elastic energies are considered. The experimental results obtained here show promising potential for nonvolatile DW-motion devices in terms of reducing device

TABLE I. Scaling property of critical width W_{crit} derived by the model with $\zeta = 1$ and 2/3 together with the experimental result.

N	t_{mag}	σ_{DW}	Experiment	$\zeta = 1$ ($\propto \sigma_{DW}$)	$\zeta = 2/3$ ($\propto {\sigma_{DW}}^{5/12} t_{mag}^{-1/3}$)
2	1	1	1	1	1
4	1.86	0.80	~0.7	0.80	0.74
6	2.71	0.74	~0.5	0.74	0.63

TABLE II. Scaling property of energy barrier E at $W = W_{crit}$ derived by the model with $\zeta = 1$ and 2/3 together with the experimental result.

N	t_{mag}	σ_{DW}	Experiment	$\zeta = 1$ ($\propto \sigma_{DW}^2\, t_{mag}$)	$\zeta = 2/3$ ($\propto \sigma_{DW}^{1/4}$)
2	1	1	1	1	1
4	1.86	0.80	~0.9	1.17	0.94
6	2.71	0.74	~0.7	1.49	0.93

size, and the findings extracted from the experiment will allow us to accurately design the nonvolatility of the devices.

ACKNOWLEDGMENTS

This work was supported by the FIRST program of JSPS, R&D for Next-Generation Information Technology of MEXT, ImPACT Program of CSTI, the R&D Subsidiary Program for Promotion of Academia-Industry Cooperation of METI, and a Grant-in-Aid for Young Scientists (B), No. 24740247, from MEXT, Japan. The authors wish to thank M. Yamanouchi, H. Sato, S. Ikeda, and F. Matsukura for fruitful discussions, and I. Morita, Y. Iwami, T. Hirata, H. Iwanuma, Y. Kawato, K. Goto, and C. Igarashi for their technical support.

APPENDIX

In the main body, we derive the scaling relation between the critical width W_{crit}, energy barrier E, and the magnetic layer thickness t_{mag} by assuming that a semicircle-shaped subvolume with a diameter of $\hat{W}$ triggers the depinning under a magnetic field H. Here we derive the scaling relation by assuming another shape of the subvolume and compare with the experimental results.

According to the theory of creep motion of DW, the displacement u for a segment of DW $\hat{W}$ is expressed as

$$u(\hat{W}) \propto \left(\frac{\hat{W}}{W_L}\right)^{\zeta}, \tag{A1}$$

where W_L is the Larkin length, given as $W_L = ({\sigma_{DW}}^2\, {t_{mag}}^2\, \xi^2/\Delta)^{1/3}$, where ξ is the characteristic length of the disorder potential and Δ is the pinning strength of the disorder. ζ is referred to as the roughness exponent. While $\zeta = 1$ [34,35] leads to the scaling relation described in the main body, here we use $\zeta = 2/3$, which is the case for the random bond disorder model of an elastic line interface in a two-dimensional disordered medium [23,36–38]. To simply evaluate the scaling properties, here we neglect numerical factors. In the case that $\zeta = 2/3$, the Zeeman energy ε_Z and DW elastic energy ε_{DW} are given as

$$\varepsilon_Z = -A\hat{W}^{5/3} \quad \left(A = \frac{M_S H {t_{mag}}^{5/9}}{{\sigma_{DW}}^{4/9}}\right), \tag{A2}$$

$$\varepsilon_{DW} = B\hat{W}^{1/3} \quad (B = {\sigma_{DW}}^{1/9} {t_{mag}}^{1/9}). \tag{A3}$$

The critical condition $\partial\varepsilon_{tot}/\partial\hat{W} = 0$ leads to the scaling relation of W_{crit} and E at $W = W_{crit}$ as

$$W_{crit} = \left(\frac{B}{A}\right)^{3/4} = \left(\frac{1}{M_S H}\right)^{3/4} \frac{{\sigma_{DW}}^{5/12}}{{t_{mag}}^{1/3}}, \tag{A4}$$

$$E = \varepsilon_{tot}(\hat{W} = W_{crit}) = \left(\frac{B^5}{A}\right)^{1/4} = \left(\frac{1}{M_S H}\right)^{1/4} {\sigma_{DW}}^{1/4}. \tag{A5}$$

Tables I and II, respectively, summarize the scaling relation of W_{crit} and E along with the experimental results. Closer agreement with the experimental results can be seen in the model with $\zeta = 2/3$ than in the model with $\zeta = 1$. Further agreement may be obtained by taking into account the t_{mag} dependence of ξ and Δ. If ξ decreases and Δ increases as t_{mag} increases, the discrepancy between the analytical model and experiment is found to be more reduced.

[1] H. Ohno, T. Endoh, T. Hanyu, N. Kasai, and S. Ikeda, in *2010 IEEE International Electron Devices Meeting, San Francisco, CA* (IEEE, New York, NY, 2010), p. 9.4.1.

[2] N. Sakimura, Y. Tsuji, R. Nebashi, H. Honjo, A. Morioka, K. Ishihara, K. Kinoshita, S. Fukami, S. Miura, N. Kasai, T. Endoh, H. Ohno, T. Hanyu, and T. Sugibayashi, in *2014 IEEE International Solid-State Circuits Conference, San Francisco, CA* (IEEE, New York, NY, 2014), p. 184.

[3] R. Takemura, T. Kawahara, K. Miura, H. Yamamoto, J. Hayakawa, N. Matsuzaki, K. Ono, M. Yamanouchi, K. Ito, H. Takahashi, S. Ikeda, H. Hasegawa, H. Matsuoka, and H. Ohno, IEEE J. Solid-State Circuits **45**, 869 (2010).

[4] H. Sato, M. Yamanouchi, K. Miura, S. Ikeda, H. D. Gan, K. Mizunuma, R. Koizumi, F. Matsukura, and H. Ohno, Appl. Phys. Lett. **99**, 042501 (2011).

[5] J. Z. Sun, R. P. Robertazzi, J. Nowak, P. L. Trouilloud, G. Hu, D. W. Abraham, M. C. Gaidis, S. L. Brown, E. J. O'Sullivan, W. J. Gallagher, and D. C. Worledge, Phys. Rev. B **84**, 064413 (2011).

[6] L. Berger, J. Appl. Phys. **55**, 1954 (1984).

[7] D. A. Allwood, G. Xiong, C. C. Faulkner, D. Atkinson, D. Petit, and R. P. Cowburn, Science **309**, 1688 (2005).

[8] S. S. P. Parkin, M. Hayashi, and L. Thomas, Science **320**, 190 (2008).

[9] S. Fukami, T. Suzuki, K. Nagahara, N. Ohshima, Y. Ozaki, S. Saito, R. Nebashi, N. Sakimura, H. Honjo, K. Mori, C. Igarashi, S. Miura, N. Ishiwata, and T. Sugibayashi, in *2009 Symposium on VLSI Technology*, Kyoto, Japan (Japan Society of Applied Physics and IEEE, New York, 2009), p. 230.

[10] M. Yamanouchi, D. Chiba, F. Matsukura, T. Dietl, and H. Ohno, Phys. Rev. Lett. **96**, 096601 (2006).

[11] L. Thomas, M. Hayashi, X. Jiang, R. Moriya, C. Rettner, and S. S. P. Parkin, Nature (London) **443**, 197 (2006).

[12] T. Koyama, D. Chiba, K. Ueda, K. Kondou, H. Tanigawa, S. Fukami, T. Suzuki, N. Ohshima, N. Ishiwata, Y. Nakatani, K. Kobayashi, and T. Ono, Nat. Mater. **10**, 194 (2011).

[13] K. S. Ryu, L. Thomas, S. H. Yang, and S. S. P. Parkin, Nat. Nanotechnol. **8**, 527 (2013).

[14] S. Emori, U. Bauer, S. M. Ahn, E. Martinez, and G. S. Beach, Nat. Mater. **12**, 611 (2013).

[15] S. Fukami, M. Yamanouchi, S. Ikeda, and H. Ohno, Nat. Commun. **4**, 2293 (2013).

[16] J. Attané, D. Ravelosona, A. Marty, Y. Samson, and C. Chappert, Phys. Rev. Lett. **96**, 147204 (2006).

[17] K.-J. Kim, J.-C. Lee, S.-M. Ahn, K.-S. Lee, C.-W. Lee, Y. J. Cho, S. Seo, K.-H. Shin, S.-B. Choe, and H.-W. Lee, Nature (London) **458**, 740 (2009).

[18] K.-J. Kim, J. Ryu, G.-H. Gim, J.-C. Lee, K.-H. Shin, H.-W. Lee, and S.-B. Choe, Phys. Rev. Lett. **107**, 217205 (2011).

[19] S. Fukami, T. Suzuki, K. Nagahara, N. Ohshima, and N. Ishiwata, J. Appl. Phys. **108**, 113914 (2010).

[20] K.-J. Kim, R. Hiramatsu, T. Koyama, K. Ueda, Y. Yoshimura, D. Chiba, K. Kobayashi, Y. Nakatani, S. Fukami, M. Yamanouchi, H. Ohno, H. Kohno, G. Tatara, and T. Ono, Nat. Commun. **4**, 2011 (2013).

[21] J.-P. Tetienne, T. Hingant, J.-V. Kim, L. Herrera Diez, J.-P. Adam, K. Garcia, J.-F. Roch, S. Rohart, A. Thiaville, D. Ravelosona, and V. Jacques, Science **344**, 1366 (2014).

[22] J. Pommier, P. Meyer, G. Pénissard, J. Ferré, P. Bruno, and D. Renard, Phys. Rev. Lett. **65**, 2054 (1990).

[23] S. Lemerle, J. Ferré, C. Chappert, V. Mathet, T. Giamarchi, and P. Le Doussal, Phys. Rev. Lett. **80**, 849 (1998).

[24] J. Wunderlich, D. Ravelosona, C. Chappert, F. Cayssol, V. Mathet, J. Ferré, J.-P. Jamet, and A. Thiaville, IEEE Trans. Magn. **37**, 2104 (2001).

[25] F. Cayssol, D. Ravelosona, J. Wunderlich, C. Chappert, V. Mathet, J.-P. Jamet, and J. Ferré, J. Magn. Magn. Mater. **240**, 30 (2002).

[26] F. Cayssol, D. Ravelosona, C. Chappert, J. Ferré, and J. P. Jamet, Phys. Rev. Lett. **92**, 107202 (2004).

[27] S.-W. Jung, W. Kim, T.-D. Lee, K.-J. Lee, and H.-W. Lee, Appl. Phys. Lett. **92**, 202508 (2008).

[28] S. Fukami, T. Suzuki, N. Ohshima, K. Nagahara, and N. Ishiwata, J. Appl. Phys. **103**, 07E718 (2008).

[29] H. Tanigawa, T. Suzuki, S. Fukami, K. Suemitsu, N. Ohshima, and E. Kariyada, Appl. Phys. Lett. **102**, 152410 (2013).

[30] Y. Yoshimura, T. Koyama, D. Chiba, Y. Nakatani, S. Fukami, M. Yamanouchi, H. Ohno, K.-J. Kim, T. Moriyama, and T. Ono, Appl. Phys. Express **7**, 033005 (2014).

[31] B. Raquet, M. D. Ortega, M. Goiran, A. R. Fert, J. P. Redoules, R. Mamy, J. C. Ousset, A. Sdaq, and A. Khmou, J. Magn. Magn. Mater. **150**, L5 (1995).

[32] J. A. Cape and G. W. Lehman, J. Appl. Phys. **42**, 5732 (1971).

[33] S. Fukami, M. Yamanouchi, Y. Nakatani, K. J. Kim, T. Koyama, D. Chiba, S. Ikeda, N. Kasai, T. Ono, and H. Ohno, J. Appl. Phys. **115**, 17D508 (2014).

[34] M. Yamanouchi, J. Ieda, F. Matsukura, S. E. Barnes, S. Maekawa, and H. Ohno, Science **317**, 1726 (2007).

[35] A. Kirilyuk, J. Ferré, V. Grolier, J. P. Jamet, and D. Renard, J. Magn. Magn. Mater. **171**, 45 (1997).

[36] D. A. Huse and C. L. Henley, Phys. Rev. Lett. **54**, 2708 (1985).

[37] D. A. Huse, C. L. Henley, and D. S. Fisher, Phys. Rev. Lett. **55**, 2924 (1985).

[38] M. Kardar and D. R. Nelson, Phys. Rev. Lett. **55**, 1157 (1985).